Available online at www.sciencedirect.com
ScienceDirect
Catalysis Today 125 (2007) 282–290
CATALYSIS TODAY
www.elsevier.com/locate/cattod

Effect of palladium on sulfur resistance in Pt–Pd bimetallic catalysts

Hong Jiang *, Hong Yang, Randall Hawkins, Zbigniew Ring

National Centre for Upgrading Technology, Devon, Alberta, Canada T9G 1A8

Available online 16 January 2007

Abstract

The interactions of H_2 and H_2S molecules with Pt–Pd bimetallic catalysts were investigated at the molecular level using a DFT (density functional theory) approach to better understand the structures and properties of active sites, and the relations between structural changes and sulfur resistance. It was found that when alloying the Pt catalyst with a small amount of Pd at a particular surface atomic ratio range, both H_2 and H_2S showed different adsorption properties compared to those on monometallic Pt or Pd catalyst. The adsorptions of both H_2 and H_2S were enhanced, but the adsorption energy of H_2 increased more than that of H_2S, indicating that the adsorption of H_2S became less favorable compared with H_2 on the bimetallic Pt–Pd catalyst surface. The desorption energy of hydrogen from monometallic Pt or Pd, as well as bimetallic Pt–Pd supported on zeolite, were calculated by temperature-programmed desorption (TPD), the values were compared against the DFT results to explain experimentally and theoretically why the bimetallic Pt–Pd catalyst has better sulfur resistance than monometallic Pt catalyst.

Keywords: Platinum; Palladium; TPD; DFT; Adsorption energy; Sulfur resistance

1. Introduction

Supported platinum catalysts are well known for their high activities for hydrogenation, paraffin hydroisomerization/hydrocracking and naphtha reforming. These catalysts, however, are easily poisoned by sulfur compounds, such as H_2S and organic sulfur-containing molecules. It is commonly accepted that the best way to improve sulfur-resistance of noble metal catalysts is to modify their electronic properties. Catalysts containing electron-deficient metal atoms on the surface are more sulfur resistant. Electron-deficient species can be formed either by the interaction of metal and acid sites on the support or by bimetallic interaction. Many processes in the petrochemical and fine-chemicals synthesis industry are carried out over supported bimetallic catalysts. Recently, much attention has been paid to Pd–Pt bimetallic catalyst supported on γ-Al_2O_3, acidic zeolites, MCM-41, or amorphous SiO_2–Al_2O_3 [1–4]. These platinum–palladium bimetallic catalysts perform better than either of the monometallic catalysts in selectivity and resistance to poisoning as well as activity. The two highly dispersed active metals, Pt and Pd, are thought to exist as an alloy or as bimetallic clusters, and the high sulfur tolerance is attributed to structural and electronic effects rather than the degree of metal dispersion in bimetallic Pt–Pd catalysts.

Yasuda et al. confirmed that the coexistence of Pt and Pd in USY zeolite strongly enhances tetralin hydrogenation and improves sulfur tolerance. They pointed out that the high sulfur tolerance of the Pd–Pt system was attributed to structural and electronic effects rather than to the degree of metal dispersion [5]. Matsubayashi et al. also studied the Pt–Pd bimetallic catalysts supported on USY zeolites. They provided the evidence of Pt–Pd ionic interaction by means of EXAFS [6]. Lee and Rhee investigated the sulfur tolerance of bimetallic Pd–Pt/H-Beta catalysts for the isomerization of *n*-hexane in the presence of thiophene [7]. They confirmed that Pd–Pt/H-Beta catalysts were more sulfur resistant than Pd/H-Beta and Pt/H-Beta, regardless of the preparation method and the Pd/Pt atomic ratio. They suggested that the Pd–Pt bimetallic interaction brought about the increase in the amount of electron-deficient metal sites, which improved the sulfur tolerance by reducing irreversible electrophilic sulfur adsorption. Navarro et al. compared silica–alumina supported Pt, Pd, and Pt–Pd catalysts for the hydrogenation of toluene and naphthalene in the presence of dibenzothiophene [8]. The Pt–Pd catalysts showed higher sulfur resistance and activity with respect to their

* Corresponding author. Tel.: +1 780 987 8785; fax: +1 780 987 5349.
E-mail address: hojiang@nrcan.gc.ca (H. Jiang).

0920-5861/$ – see front matter.
doi:10.1016/j.cattod.2006.11.026

monometallic (Pt and Pd) counterparts in hydrogenation of toluene and naphthalene. The higher sulfur resistance and activity of Pt–Pd catalysts were explained due to the formation of electron-deficient platinum species formed from Pt–Pd particles. Rades et al. demonstrated a strong alloying effect between Pt and Pd supported on NaY zolite by hydrogen chemisorption and proton NMR of sorbed species [9]. However, these practical attempts failed to provide direct evidence on the structural and electronic changes in Pt–Pd bimetallic catalysts: how these two metal components coexist and interact, in which way the energy and charge change on the catalyst surface, how the structural and electronic changes affect the adsorption of molecules onto the catalyst surface. In fact, due to the lack of suitable experimental technique, it is hard to give clear explanations experimentally unless further progress is made.

On the other hand, molecular modeling and simulation have made important contributions to provide a means to understand and to predict the interactions between atoms and molecules, as well as model chemical reactions on a microscopic scale. Many DFT calculations have been done to better understand the behavior of molecules/atoms on metal catalysts and the reaction mechanisms at the molecular level. Among those computational attempts, the interaction of hydrogen with metal surfaces has been studied for a long time, especially the adsorption process of hydrogen on metal surfaces. In hydrogenation/dehydrogenation reactions, for example, adsorption of hydrogen may dominate the direction of the reaction in some cases. Therefore, the adsorption of hydrogen on metal surfaces plays a very important role in understanding the dynamics of various reactions. Recently Olsen et al. reported their DFT investigations of H atom adsorbed on platinum metal surfaces by potential energy surface (PES) [10] and Watson et al. by Vienna *ab initio* Simulation Program (VASP) [11]. Paul and Sautet have studied the adsorption of H atoms on Pd(1 1 1) by computing the exchange and correlation energies [12]. Dong et al. also studied the adsorption of H atoms on Pd(1 1 1) by DFT method using VASP [13]. Meanwhile, the adsorptions of H_2S on pure platinum and palladium metal surfaces have also been studied by DFT method. Alfonso et al. found that molecular adsorption of H_2S on Pt(1 1 1) or Pd(1 1 1) surface was stable with H_2S binding preferentially at atop site [14,15]. These computational investigations have provided us the detailed information about the adsorption behavior of hydrogen or H_2S on monometallic metal surfaces. The adsorption properties of hydrogen or H_2S on Pt–Pd bimetallic metal surfaces, on the other hand, are expected to be different from those on monometallic metal surfaces due to the interaction between the two metal components Pt and Pd. The changes in adsorption properties of H_2 and H_2S on Pt–Pd bimetallic surface, such as the adsorption energies and the preferable adsorption sites, will be a key to better understanding the high sulfur tolerance of Pt–Pd bimetallic catalyst. Unfortunately, the adsorptions of either H_2 or H_2S on Pt–Pd bimetallic metal surfaces have not been studied theoretically or experimentally so far.

The objective of our work is to investigate the effect of Palladium on sulfur resistance in Pt–Pd bimetallic catalysts theoretically as well as experimentally. Theoretical results from our DFT calculations will be summarized and discussed through surface structural and electronic changes, properties of active sites, as well as the relations between structure changes and sulfur resistance. The adsorption and dissociation of H_2 and H_2S on monometallic Pt and Pd catalysts will also be discussed for comparison. Meanwhile, experimentally the interactions of hydrogen with Pt, Pd or Pt–Pd supported on H-Y zeolite were also investigated by TPD analysis. We will discuss the binding state of hydrogen on both monometallic and bimetallic surfaces by analyzing their TPD profiles, and also discuss the difference of kinetic parameters from monometallic and bimetallic surfaces by TPD kinetic analysis. Eventually, the experimental results from our TPD will be summarized and discussed by comparing with theoretical results from our simulation.

2. Computational methods

2.1. DFT calculations

The DFT calculations were performed using Material Studio DMol^3 from Accelrys (version 3.1) on a personal computer. The double-numerical plus *d* functions (DND) and the effective core potential (ECP) were used for all the calculations. The DND basis set includes one numerical function for each occupied atomic orbital and a second set of functions for valence atomic orbitals, plus a polarization *d* function on all atoms. Becke exchange plus Perdew, Burke, and Ernzerhof exchange functional (GGA-PBE) are used in all calculations. The calculation quality control settings are medium for all geometry optimizations, and the optimization convergence thresholds for energy change, maximum force, and maximum displacement between optimization cycles are 0.00002 Ha, 0.004 Ha/Å, and 0.005 Å, respectively. A *k*-point set of ($4 \times 4 \times 1$) and spin polarization were applied to all calculations.

2.2. Computational models

A (2×2) surface unit cell with a slab of four layers thickness (16 metal atoms) was employed to model adsorption of H_2 and H_2S on (1 1 1) metal surfaces. The slab was repeated periodically with a 10 Å of vacuum region between the slabs in the *y* direction. Only one molecule of H_2 or H_2S was assumed to adsorb on one side of the slab (the coverage is 1/4 monolayer). H_2 or H_2S and the two top layers of metal were allowed to relax in all the geometry optimization calculations. For the Pt–Pd bimetallic surface, Pd substituted Pt(1 1 1) surfaces are chosen as our computational models described as Pt(1 1 1)–*n*Pd, $n = 1$, 2, 3, 4. Pt and Pd atomic ratios on the first surface layer, Pt/Pd were 3/1, 2/2, 1/3 and 0/4, respectively. The slab models of pure (1 1 1) metal surface and four bimetallic surfaces are shown in Fig. 1 (only the most stable surface structure was considered at different Pt and Pd atomic ratio).

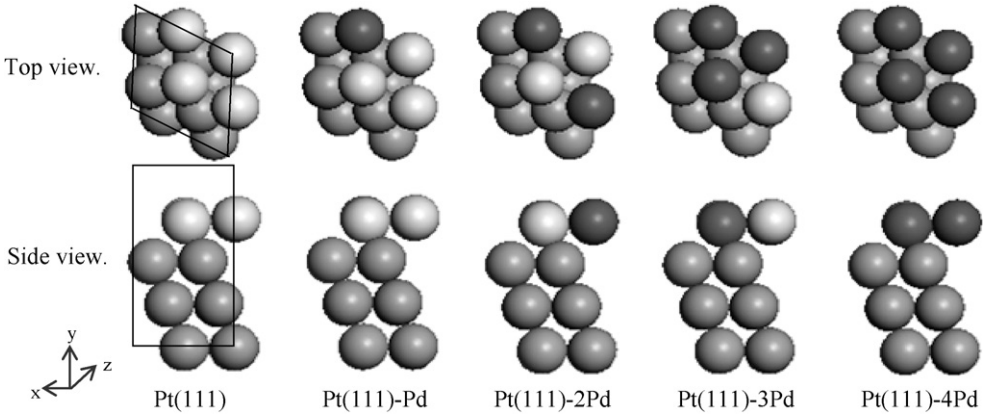

Fig. 1. Side and top views of five slab models used for DFT calculation. Darker circles on top layer correspond to Pd atoms; lighter circles correspond to Pt atoms.

The adsorption energy of H_2 ($E_{ads}(H_2)$) is calculated from

$$E_{ads}(H_2) = E(H_2/\text{surface}) - E(H_2) - E(\text{surface}) \quad (1)$$

where $E(H_2/\text{surface})$ [16] is the total energy of the surface with adsorbed H_2; $E(H_2)$ is the total energy of the free H_2 molecule and E(surface) is the total energy of the clean metal surface. With this definition, a negative E_{ads} corresponds to a stable adsorption implying that dissociate desorption from gas-phase H_2 is thermodynamically favorable. Similarly, the adsorption energy of H_2S (E_{ads} (H_2S)) is calculated according to the following equation:

$$E_{ads}(H_2S) = E(H_2S/\text{surface}) - E(H_2S) - E(\text{surface}) \quad (2)$$

3. Experimental methods

3.1. Catalyst preparation

All catalysts were prepared by incipient wetness impregnation of the supports using distilled water as solvent. CBV780 (H-Y Zeolite, Zeolyst International, BET surface area: 780 m^2/g, SiO_2/Al_2O_3 mole ratio: 80) was used as the catalyst support. $Pt(NH_3)_4Cl_2$ and $Pd(NH_3)_4Cl_2$ (Johnson Matthey) were used as metal precursors. The Pt–Pd/CBV780 bimetallic catalysts were prepared by coimpregnation method. The platinum loading was maintained constant at 1.0 wt.% for all catalysts and the palladium loading was varied from 0.2 to 1.7 wt.% to get mole ratio of Pt/Pd = 3/1, 2/2 and 1/3. Following the impregnation step, the impregnated catalysts were dried at room temperature for 72 h, and then calcined in air at 400 °C for 2 h. The catalyst denoted as Pt-0.2Pd/CBV780 (Pt/Pd = 3/1) means 1.0 wt.% Pt and 0.2 wt.% Pd supported on CBV780. Similarly, Pt-0.5Pd/CBV780 (Pt/Pd = 2/2) is denoted as 1.0 wt.% Pt and 0.5 wt.% Pd supported on CBV780, Pt-1.7Pd/CBV780 (Pt/Pd = 1/3) is denoted as 1.0 wt. % Pt and 1.7 wt.% Pd supported on CBV780.

3.2. Temperature-programmed reduction

TPR/TPD was carried out in an automated catalyst characterization system: AutoChem II 2920 from Micromeritics. About 200 mg of sample was used in each TPR/TPD run. Sample was placed into a quartz tube reactor, which was externally heated by a tube furnace. Prior to TPR, all samples were dried for 90 min at 300 °C and cooled down to room temperature in argon stream with flow rate of 50 ml/min. Then, the samples were slowly heated to 400 °C at a rate of 2 °C/min, and reduced for 5 h at 400 °C with a stream of hydrogen/argon (10% of hydrogen by volume) at a flow rate of 50 ml/min. The amount of consumed hydrogen during reduction was detected with thermal conductivity detector (TCD).

3.3. Temperature-programmed desorption

After the reduction step, the following two procedures were carried out for different TPD analysis.

For pulse chemisorption/TPD analysis, after completing the reduction, the catalysts were purged with a stream of argon (flow rate, 50 ml/min) for 2 h at 450 °C to desorb all the adsorbed hydrogen. Then the hydrogen was injected into the reactor at room temperature, and after completing the adsorption, the reactor was heated to 700 °C with a linear ramping rate of 10 °C/min in an argon flow of 50 ml/min. The initial coverage of hydrogen was controlled by the pulses injected to the reactor.

For TPD analysis of saturate hydrogen (all available surface metal atoms are completely occupied by hydrogen atoms, i.e., coverage = 1), after completing the reduction, the catalysts were cooled down to room temperature and kept in a stream of hydrogen/argon (10% hydrogen) at a flow rate of 50 ml/min for 2 h to saturate the surface. After completing the adsorption, the reactor was heated to 700 °C in an argon flow of 50 ml/min with different ramping rates between 4 and 20 °C/min. We performed TPD with different carrier argon gas flow rates between 20 and 90 ml/min. It was found that readsorption of hydrogen could be neglected when the flow rate of argon carrier gas was over 50 ml/min. Therefore, the argon flow rate was fixed at 50 ml/min for all TPD analysis in this work. The amounts of desorbed hydrogen were monitored with TCD.

4. Computational results and discussion

4.1. Adsorption of H_2, H_2S on Pt(1 1 1) and Pd(1 1 1) monometallic surfaces

When a molecule or atom (adsorbate) adsorbs on an atop site, the adsorbate is bonded to only one surface metal atom. Similarly, for a two-fold bridge site, adsorbate is bonded to two surface metal atoms. For a three-fold hollow fcc (face centered cubic) and hcp (hexagonal close packed) sites, adsorbate is sitting in the triangular surface plane and is bonded to three surface metal atoms. In this work, adsorption of H_2, H_2S on Pt(1 1 1) and Pd(1 1 1) surfaces was examined on the above four adsorption sites: atop, bridge, fcc, and hcp. Adsorption energies at preferred adsorption sites are listed in Table 1. Our results show that H_2 dissociated at all adsorption sites on both Pt(1 1 1) and Pd(1 1 1) surfaces. The most preferable sites are the same for Pt(1 1 1) and Pd (1 1 1): the three-fold fcc hollow site, over which the highest adsorption energies of −16.8 and −24.2 kcal/mol were obtained, respectively. However, after H_2 dissociated, two H atoms adsorbed at atop sites on Pt(1 1 1), while, on Pd(1 1 1), the H atoms adsorbed at fcc and hcp sites. Olsen et al. have investigated the corrugation of H_2/Pt(1 1 1) potential energy surface(PES) by using DFT-GGA method. They concluded that the atop site was slightly preferred by H atoms as compared to other adsorption sites [10]. Paul and Sautet have studied the adsorption of H atoms on Pd(1 1 1) by computing the exchange and correlation energies. They found that H atoms preferred to adsorb on an fcc hollow site on the Pd(1 1 1) surface [12]. Dong et al. also performed DFT-GGA computation to study the interaction of atomic hydrogen with the Pd(1 1 1) surface. They confirmed that H atoms always adsorbs in the highest coordination site, i.e., the three-fold hollow site [13]. Our calculations are in good agreement with these previous DFT calculations.

For the adsorption of H_2S on Pt(1 1 1) and Pd(1 1 1) surfaces, the optimized H_2S always positioned on the atop site, indicating that the atop site is favorable for H_2S on both Pt(1 1 1) and Pd(1 1 1) surfaces. In this configuration, H_2S lies nearly parallel to the surface with one S–H bond directed toward an hcp site, whereas the other one points towards a bridge site, and the H–S–H internal angle remains unchanged from its gas phase value of 92°. The S–Pt and S–H distances at this site are 2.36 and 1.37 Å on Pt(1 1 1), 2.35 and 1.37 Å on Pd(1 1 1), respectively. These results agree well with theoretical studies of Alfonso et al. [14,15]. Experimentally, however, H_2S dissociates quickly on both Pt(1 1 1) and Pd(1 1 1) surfaces at room temperature, giving rise to adsorbed atomic S species [17,18]. Our calculation and previous theoretical studies [14,15] indicated that molecular adsorption of H_2S on both Pt(1 1 1) and Pd(1 1 1) is energetically favorable. To better understand the interaction between the S-containing molecule and the metal surface, we calculated the adsorption energy of the S atom on Pt(1 1 1) and Pd(1 1 1) surfaces to compare with adsorption of H_2. On both Pt(1 1 1) and Pd (1 1 1) surfaces, fcc is the most favorable site for the S atom. The S–Pt and S-Pd distances at the optimized structures are 2.31 and 2.28 Å, respectively. In this configuration, S atoms will interact with three metal surface atoms, forming a strong binding which will block the dissociative adsorption of H_2 because both the S atom and H_2 molecule prefer to adsorb on the fcc site. Therefore, the sulfur resistant bimetallic catalyst surfaces have to provide different favorable adsorption sites for the H_2 and S atom such that the adsorbed S atoms do not block the adsorption of H_2 molecule; or increase the adsorption energy of H_2 so that the dissociative adsorption of H_2 will become more competitive to the adsorption of H_2S.

4.2. Adsorption of H_2, H_2S on Pt(1 1 1)-nPd bimetallic surface

The adsorption properties of H_2, H_2S and S atom on Pt(1 1 1) and Pd(1 1 1) surfaces from our calculations reached a good agreement with previous DFT calculations. This demonstrated the reliability and proper design of our DFT calculation, which enables us to extend this approach to bimetallic catalysts.

In this study, the adsorption energies of the H_2 and H_2S molecules as well as the S atom on Pt(1 1 1)-nPd bimetallic surfaces were calculated to compare with those on Pt(1 1 1) and Pd(1 1 1) surfaces. The same as on monometallic surfaces, four adsorption sites—atop, bridge, fcc, and hcp—were examined and results are listed in Table 2.

When one Pt atom on the top layer of Pt(1 1 1) surface was replaced by the Pd atom (Pt/Pd = 3/1, see Fig. 1), the adsorption energies of H_2 and H_2S, as well as the S atom on Pt(1 1 1)–Pd surface were increased as compared with those on the Pt(1 1 1) surface. However, the adsorption energies of the H_2, H_2S and S atom were decreased when the second Pt atom was replaced by Pd atom (Pt/Pd = 2/2). Lower adsorption energies were observed on Pt(1 1 1)–2Pd surface than those obtained on Pt(1 1 1)–Pd surface. As Pt/Pd decreased continuously from 2/2 to 1/3 and 0/4, the adsorption energies of H_2S and the S atom remained unchanged at −25.6 and −115.5 kcal/mol, respectively, while the adsorption energies of H_2 increased from −16.4 to −18.7 and −22.1 kcal/mol. In the case of the Pt(1 1 1)–4Pd surface (Pt/Pd = 0/4), where all the four Pt atoms at the top layer were substituted by Pd atoms, the adsorption

Table 1
Adsorption energies of H_2, H_2S and S at preferred adsorption sites on Pt(1 1 1) and Pd(1 1 1) surfaces

	H_2 molecules			H_2S molecules			S atoms		
	E_{ads} (kcal/mol)	Initial site	Final site	E_{ads}	Initial site	Final site	E_{ads}	Initial site	Final site
Pt(1 1 1)	−16.8	fcc	Atop	−23.3	Atop	Atop	−109.8	fcc	fcc
Pd(1 1 1)	−24.2	fcc	fcc, hcp	−22.1	Atop	Atop	−113.9	fcc	fcc

Table 2
Adsorption energies of H_2, H_2S and S at preferred adsorption sites on bimetallic Pt(1 1 1)–*n*Pd surfaces

	H_2 molecules			H_2S molecules			S atoms		
	E_{ads} (kcal/mol)	Initial site	Final site	E_{ads}	Initial site	Final site	E_{ads}	Initial site	Final site
Pt(1 1 1)–Pd	−74.9	B Pt–Pt	Atop Pt	−86.2	Atop Pt	Atop Pt	−177.1	fcc	fcc
Pt(1 1 1)–2Pd	−16.4	hcp	fcc	−25.6	Atop Pt	Atop Pt	−115.5	fcc	fcc
Pt(1 1 1)–3Pd	−18.7	B Pt–Pd	B Pt–Pd	−25.6	Atop Pt	Atop Pt	−115.5	fcc	fcc
Pt(1 1 1)–4Pd	−22.1	fcc	fcc, hcp	−25.6	Atop Pd	Atop Pd	−115.5	fcc	fcc

B Pt–Pd: bridge site between Pt and Pd atoms.

energies of H_2, H_2S and the S atom were not the same as those on the Pd(1 1 1) surface, which indicates that the interaction between the sublayer Pt atoms and top layer Pd atoms changed the properties on the Pt(1 1 1)–4Pd surface, compared to the Pd(1 1 1) surface. It is clear that the adsorption energy of H_2 strongly depends on the Pt and Pd atomic ratio on the surfaces, while adsorption energies of the H_2S and S atom increased only at Pt/Pd = 3/1 and kept constant at Pt/Pd < 3/1. Furthermore, the adsorption energies of H_2, H_2S and the S atom on Pt(1 1 1)–*n*Pd surfaces have maximum values at Pt/Pd = 3/1 where the adsorptions of all three were enhanced. To compare the competitive adsorptions of H_2 with H_2S and the S atom, $E_{ads}(H_2)/E_{ads}(S)$ and $E_{ads}(H_2)/E_{ads}(H_2S)$ were plotted in Fig. 2. At Pt/Pd = 3/1, the values of both $E_{ads}(H_2)/E_{ads}(S)$ and $E_{ads}(H_2)/E_{ads}(H_2S)$ were greater compared with those of Pt(1 1 1), indicating that the adsorption energy of H_2 increased more than those of H_2S and the S atom. At this point, the dissociative adsorption of H_2 becomes more competitive than that of H_2S and the S atom, i.e., the bimetallic catalyst has better sulfur resistance.

It is interesting to note that on Pt(1 1 1)–*n*Pd bimetallic surfaces with *n* = 1, 2, 3, H_2S always takes the Pt atop site, no matter what the Pt and Pd atomic ratio is. On the Pt(1 1 1)–4Pd surface, no Pt atop sites are available because all top layer Pt atoms are substituted by Pd atoms, and H_2S takes the Pd atop site instead. Therefore, H_2S prefers binding with the Pt atom rather than the Pd atom if there is a Pt atom on the top layer. This may answer the question of why the Pt catalyst is more sensitive to sulfur poisoning. Meanwhile, the S atom always has

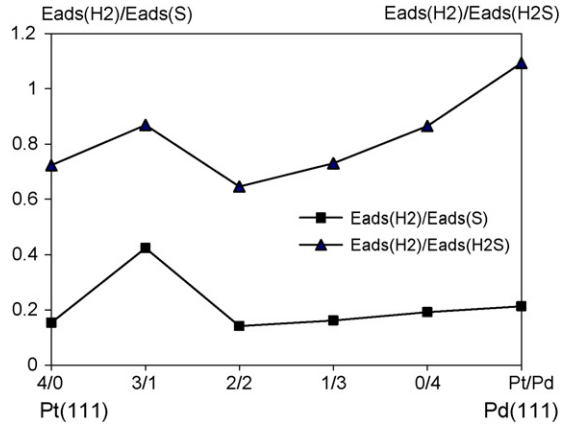

Fig. 2. Plots of $E_{ads}(H_2)/E_{ads}(S)$ and $E_{ads}(H_2)/E_{ads}(H_2S)$ as a function of Pt and Pd atomic ratio, Pt/Pd.

the fcc site as its preferred site on both Pt(1 1 1)–*n*Pd bimetallic surfaces and monometallic surfaces. However, for dissociative adsorption of H_2 on Pt(1 1 1)–*n*Pd bimetallic surfaces, the preferable adsorption sites changed as Pt and Pd atomic ratio changed. On the Pt(1 1 1)–4Pd surface, H_2 dissociates at the fcc site, then the dissociated H atoms take fcc and hcp sites as preferable sites, which is the same as on the Pd(1 1 1) surface. On the Pt(1 1 1)–Pd surface, H_2 dissociates at the bridge site (two-fold Pt–Pt), followed by the migration of dissociated H atoms to atop Pt sites. While on the Pt(1 1 1)–2Pd surface, H_2 dissociates at the hcp site with the dissociated H atoms sitting on fcc sites. On the Pt(1 1 1)–3Pd surface, H_2 dissociates at the bridge site (two-fold Pt–Pd), while the dissociated H atoms remain at two-fold Pt–Pd sites. It is clear that the preferable sites for H_2 or dissociated H atoms are different from H_2S and S atom on Pt(1 1 1)–*n*Pd surfaces (*n* = 1, 2, 3). These bimetallic surfaces provide some of the different favorable adsorption sites for H_2S and the S atom from the H_2 molecule that minimize the adsorbed H_2S and S atoms, blocking the adsorption of the H_2 molecule. Therefore, the Pt–Pd bimetallic catalysts not only provide different favorable adsorption sites for H_2 from H_2S and the S atom, but also increase the adsorption energy of H_2. The structure changes in Pt–Pd bimetallic catalysts give rise to different active sites that make the adsorption of H_2 more competitive to the adsorption of H_2S and the S atom. That is, Pt–Pd bimetallic catalysts are more sulfur resistant as comparing with their monometallic catalysts. Furthermore, charge transfers between Pt and Pd on Pt(1 1 1)–*n*Pd surfaces have been confirmed by our Mulliken analysis. These electronic and structural changes on Pt–*n*Pd bimetallic surfaces are considered to be responsible for the changes in adsorption energies, and also for the changes in preferable adsorption sites.

5. Experimental results and discussion

5.1. Reducibility of monometallic and bimetallic Pt-containing catalysts

The reducibility of Pt or Pd monometallic catalysts and Pt–Pd bimetallic catalysts was evaluated by programmed temperature reduction (TPR). TPR profiles of monometallic catalysts are shown in Fig. 3. The profile of 1%Pd/CBV780 has a reduction peak around 75 °C, which is attributed to desorption of hydrogen from the decomposition of a bulk palladium hydride formed through H-diffusion into the Pd crystallites

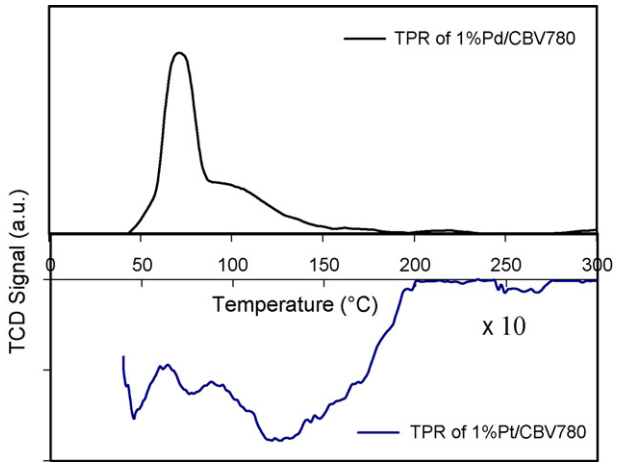

Fig. 3. TPR profiles of monometallic catalysts, 1%Pt/CBV780 and 1%Pd/CBV780.

[19]. The reduction of the Pt compound started from a lower temperature, and continued over a wider temperature range as compared with the Pd compound, suggesting the presence of several Pt species. As shown in Fig. 3, 1%Pt/CBV780 has two reduction peaks with maximum values at temperatures around 48 and 125 °C.

For Pt–Pd bimetallic catalysts, the TPR profiles are not simply the sums of the monometallic Pt and Pd samples. As shown in Fig. 4 and Table 3, all of the observed peaks were broad, indicating that the reduction was a slow process. TPR profile of Pt-0.2Pd/CBV780 (Pt/Pd = 3/1) has two peaks with maximum values at temperatures around 90 and 238 °C. Pt–1.7Pd/CBV780 (Pt/Pd = 1:3) has three peaks with maximum values at temperatures around 54, 115 and 227 °C. The maximum values of reduction peaks are not the same as any of their monometallic catalysts, suggesting that there are strong interactions between the two metal components during the reduction. As a result of the bimetallic interactions, the Pt–Pd alloy was formed to a certain degree during the reduction. As the maximum values of reduction peaks in bimetallic catalysts changed with the Pt/Pd ratio, the degree of Pt–Pd alloy formation depended on the structures of bimetallic catalysts. It is interesting to note that among all the reduction peaks from

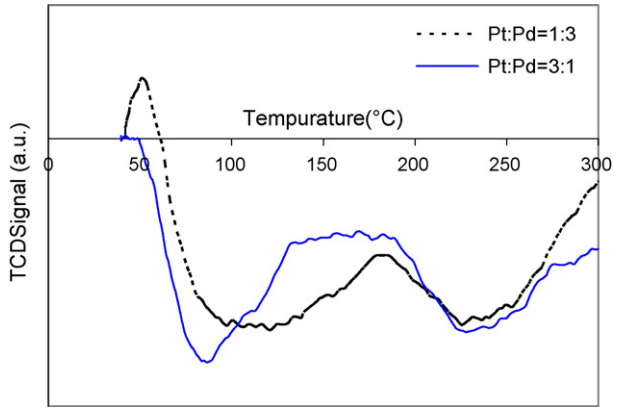

Fig. 4. TPR profiles of bimetallic catalysts, Pt–Pd/CBV780.

Table 3
Reduction temperature range of monometallic and bimetallic catalysts

Catalysts	Atomic ratio	Reduction peak range (°C)	Peak (°C)
1%Pt/780		41–68, 107–165	48, 125
1%Pt, 0.2%Pd/780	3Pt: Pd	50–134, 190–280	90, 238
1%Pt, 0.5%Pd/780	2Pt:2Pd	41–70, 75–181, 186–262	54, 127, 208
1%Pt, 1.7%Pd/780	Pt:3Pd	43–61, 61–186, 188–273	54, 115,227
1%Pd/780		45–157	75

TPR profiles of Pt–Pd bimetallic catalysts, none of them correlate to peaks from monometallic catalysts. This suggests that only bimetallic clusters existed after reduction; or, there was monometallic cluster after reduction, but the cluster was too small to show a monometallic reduction peak because of the interaction with surrounding second metal atoms. Similar meta–metal interactions in Pd-Cu systems from TPR studies have been reported by Noronha et al. [20]

5.2. TPD of hydrogen

TPD profiles of hydrogen from supported platinum [21–26], as well as from single crystal [27–30] have been investigated by many researchers. Alexeev et al. confirmed that the TPD peak centered at 120 °C represents the hydrogen chemisorbed on γ-Al_2O_3 supported Pt catalyst [25]. Miller et al. pointed out that chemisorbed hydrogen desorbed at approximately 175 °C from γ-Al_2O_3 supported Pt catalyst [23,24]. Meanwhile, Lee et al. have used TPD of hydrogen to measure the desorption energies of hydrogen on different platinum single crystal surfaces, and the calculated desorption energies were in the range17–24 kcal/mol [29,30]. TPD profile of hydrogen from palladium, on the other hand, have also been done giving rise to desorption peak temperature between 30 and 80 °C [31–34]. The desorption energies of hydrogen on different palladium single crystal surfaces from previous studies are between 20 and 24 kcal/mol [34–36].

In this work, we applied the same TPD of hydrogen procedure to both monometallic and bimetallic catalysts and also calculated/compared the kinetic parameters from our own analysts in order to minimize the experimental error. First, the relation between desorption peak position and initial coverage of hydrogen was investigated by pulse chemisorption/TPD analysis. The desorption properties of hydrogen from both monometallic and bimetallic catalysts showed the same trends. The peak temperatures decreased as initial coverage increased. This demonstrated that desorption of hydrogen from both monometallic and bimetallic catalysts are second order desorption [37–39]. To extract quantitative kinetic information, TPD of hydrogen from monometallic and bimetallic catalysts with different ramping rates were performed at saturated coverage. TPD profiles of hydrogen from 1%Pt/CBV780 and 1%Pd/CBV780 are shown in Figs. 5 and 6, respectively. The desorption peak of hydrogen from 1%Pd/CBV780 was observed at a much higher temperature than that from 1%Pt/CBV780, suggesting that the desorption of hydrogen from 1%Pd/CBV780 was not as easy as from 1%Pt/CBV780.

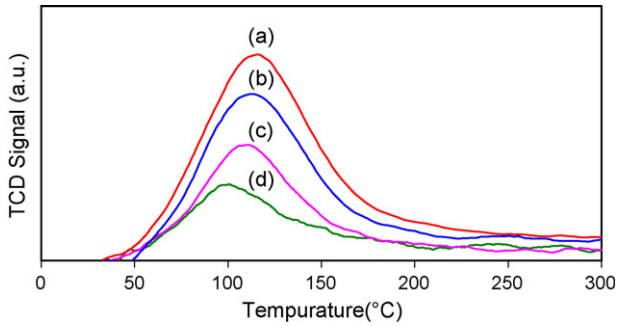

Fig. 5. TPD profiles of hydrogen from 1%Pt/CBV780. Ramping rate at (a) 16 °C/min; (b) 12 °C/min; (c) 8 °C/min; (d) 4 °C/min.

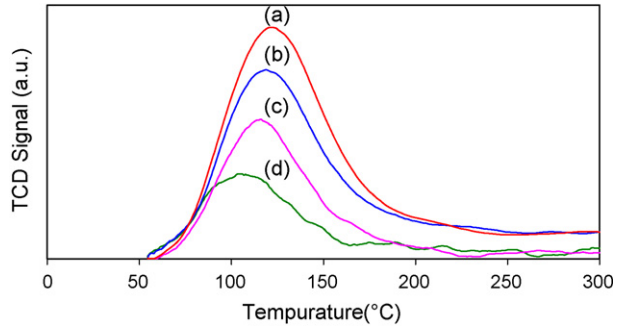

Fig. 6. TPD profiles of hydrogen from 1%Pd/CBV780. Ramping rate at (a) 16 °C/min; (b) 12 °C/min; (c) 8 °C/min; (d) 4 °C/min.

Therefore, the supported Pt catalyst has higher hydrogenation/dehydrogenation activity than that of supported Pd catalyst.

The desorption energies of hydrogen on supported Pt and Pd catalysts were calculated from the slope of Arrhenius plot ($\ln(T_{max}^2/\beta)$ versus $1/T_{max}$) of Fig. 7 using a heating rate variation method [37], and results are shown in Table 4. Desorption energy of hydrogen on 1%Pd/CBV780, 23.8 kcal/mol, was larger than that from 1%Pt/CBV780, 21.8 kcal/mol, which agrees well with previous experimental results [29,30,34–36]. TPD profiles of hydrogen from supported bimetallic Pt–Pd catalysts are shown in Fig. 8, with atomic ratio Pt/Pd = 3/1, 1/1, 1/3, respectively. Arrhenius plot is shown in Fig. 9. Desorption energies of hydrogen were calculated from Fig. 9 and results are shown in Table 4. Desorption energies of hydrogen from Pt–0.2Pd/CBV780, 33.1 kcal/mol, was larger than those from Pt–0.5Pd/CBV780 and Pt–1.7Pd/CBV780, 22.9 and 20.1 kcal/mol, respectively.

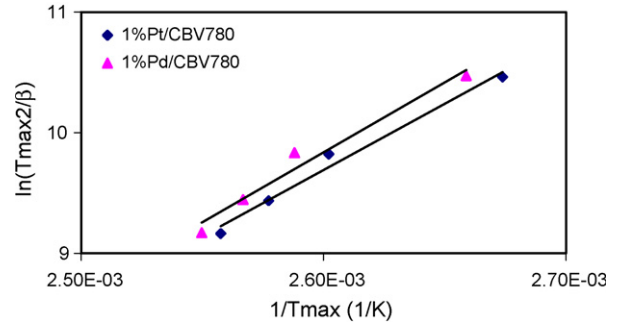

Fig. 7. Arrhenius plot ($\ln(T_{max}^2/\beta)$ vs. $1/T_{max}$) for hydrogen desorption from 1%Pt/CBV780 and 1%Pd/CBV780.

Table 4
Comparison of theoretical results from DFT and experimental results from TPD

Surface models	Atomic ratio	DFT	TPD
		E_{ads} (kcal/mol)	E_{des} (kcal/mol)
Pt(1 1 1)		−16.8	21.8
Pt(1 1 1)–Pd	3Pt:Pd	−74.9	33.1
Pt(1 1 1)–2Pd	2Pt:2Pd	−16.4	22.9
Pt(1 1 1)–3Pd	Pt:3Pd	−18.7	20.1
Pd(1 1 1)		−24.2	23.8

It should be noted that DFT calculations provide adsorption energies (negative) corresponding to the adsorption process, while TPD calculations provides desorption energies (positive) corresponding to the desorption process. The relation between the adsorption energy and desorption energy depends on the nature of adsorption/desorption process. In chemisorption, the overlap between the molecular orbitals and surface atoms occurs to form chemical bonds, which usually requires an activation energy to overcome the barrier,

$$\text{desorption energy} = -(\text{adsorption energy} + \text{activation energy}) \quad (3)$$

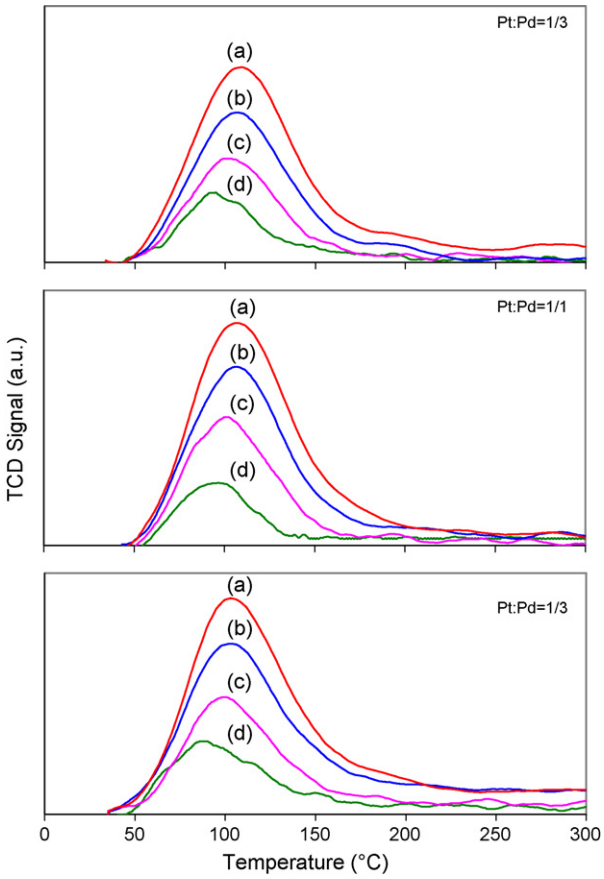

Fig. 8. TPD profiles of hydrogen from Pt–Pd/CBV780. Ramping rate at (a) 16 °C/min; (b) 12 °C/min; (c) 8 °C/min; (d) 4 °C/min.

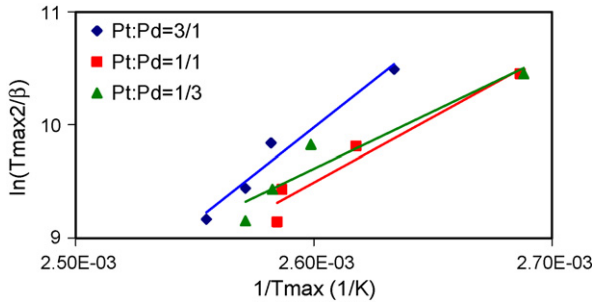

Fig. 9. Arrhenius plot ($\ln(T_{max}^2/\beta)$ vs. $1/T_{max}$) for hydrogen desorption from Pt–Pd/CBV780 bimetallic catalysts.

In the case of hydrogen molecule adsorbs on Pt or Pd surfaces, activation energy is nearly zero as comparing with the adsorption energy [40,41], resulting in

$$\text{desorption energy} \approx -\text{adsorption energy} \quad (4)$$

Therefore, in these particular cases, we can compare the absolute values of adsorption energies from DFT (negative) against desorption energies from TPD (positive). As shown in Table 4, for adsorption energies of hydrogen on monometallic Pt(1 1 1) or Pd(1 1 1) surfaces, calculations from DFT agree well with those from experimental results from TPD. While, for adsorption energies of hydrogen on bimetallic Pt–Pd catalysts, there was a gap between the experimental results and theoretical results. As already known that TPD techniques are important methods for the determination of kinetic and thermodynamic parameters of desorption processes, it provides information closely related to the catalytic properties and has been widely applied to supported catalyst in the study of adsorption–desorption kinetics. DFT theoretical approach, unfortunately, is performed based on the molecule-metal models (cluster or periodic slab) in studying of adsorption or reaction on catalyst surfaces. Even though significant progress has been made over the past decade in theoretical field, it is still not a real option to include the support (zeolite in this work) in DFT calculations because of the complexity of molecule-metal-support model, as well as the demanding for computation time. Correspondingly, in this study, we chose the molecule-metal models to study the adsorption–desorption kinetics as our first approach. As mentioned above, the molecule-metal models used in DFT calculation was a simplified model in the characteristics of hydrogen adsorption on supported metal catalysts, which neglect the interactions between the metal and support. On supported bimetallic catalysts, not only the metal–support interactions, but also the metal–metal interactions are involved, which make the adsorption process of hydrogen more complicate. Furthermore, experimentally, desorption process of hydrogen is affected by many other factors including particle size, reduction temperature, ramping rate and hydrogen gas flow rate during the reduction, etc. As a result, there was a gap between the experimental results from TPD and theoretical results from DFT in bimetallic system.

6. Conclusions

Adsorption of H_2, H_2S and S atom on Pt(1 1 1)–*n*Pd bimetallic surfaces were investigated theoretically by DFT computation. Surface structural and electronic changes, properties of active sites, as well as the relations between structure changes and sulfur resistance on Pt–Pd bimetallic surfaces are discussed. The bimetallic surfaces not only enhance the adsorption of the H_2, but also provide different favorable adsorption sites that make the dissociative adsorption of H_2 more competitive on the bimetallic surface. These DFT results provided us a theoretical explanation why Pt–Pd bimetallic catalysts are more sulfur resistant as compared with their monometallic catalysts.

Desorption of hydrogen on supported Pt and Pd monometallic catalysts as well as on Pt–Pd bimetallic catalysts are investigated experimentally by TPD. The desorption energies of hydrogen are calculated from TPD kinetic analysis and compared with theoretical results from DFT calculations. The calculated adsorption energies from DFT are within 6 kcal/mol of TPD experimental values except the case of bimetallic catalyst Pt/Pd = 3/1. This general agreement between experimental and theoretical results suggests that the present theoretical methods reasonably predict the interactions of hydrogen with metal surface.

Acknowledgements

Partial funding for this work has been provided by the Canadian Program for Energy Research and Development (PERD) and the Alberta Research Council. The authors wish to thank Norman Sacuta for editorial assistance.

References

[1] J.R. Chang, S.L. Chang, J. Catal. 176 (1998) 42.
[2] C. Song, A.D. Schmitz, Energy & Fuels 11 (1997) 656.
[3] A. Corma, A. Martínez, V. Martínez-Soria, J. Catal. 169 (1997) 480.
[4] M. Vaarkamp, W. Dijkstra, B.H. Reesink, P.H. Berben, Am. Chem. Soc., Div. Petrol. Chem. Prepr. 43 (1998) 77.
[5] H. Yosuda, Y. Yoshimura, Catal. Lett. 46 (1997) 43.
[6] N. Matsubayashi, H. Yasuda, M. Imamura, Y. Yoshimura, Catal. Today 45 (1998) 375.
[7] J.K. Lee, H.K. Rhee, J. Catal. 177 (1998) 208.
[8] R.M. Navarro, B. Pawelec, J.M. Trejo, R. Mariscal, J.L.G. Fierro, J. Catal. 189 (2000) 184.
[9] T. Rades, M. Polisset-Thfoin, J. Fraissard, Topics Catal. 11/12 (2000) 283.
[10] R.A. Olsen, G.J. Kroes, E.J. Baerends, J. Chem. Phys. 111 (1999) 11155.
[11] G.W. Watson, R.P.K. Wells, D.J. Willock, G.J. Hutchings, Chem. Commun. (2000) 705.
[12] J.F. Paul, P. Sautet, Surf. Sci. 356 (1996) 403.
[13] W. Dong, V. Ledentu, P. Sautet, A. Eichler, J. Hafner, Surf. Sci. 411 (1998) 123.
[14] D.R. Alfonso, A.V. Cugini, D.C. Sorescu, Catal. Today 99 (2005) 315.
[15] A. Michaelides, P. Hu, J. Chem. Phys. 115 (2001) 8570.
[16] Total energy E(H2/surface), can also be defined as E(2H/surface) for H2 molecules that dissociate and adsorb as atoms at preferred sites on the surface.
[17] S. Speller, T. Rauch, J. Bömermann, P. Bormann, W. Heiland, Surf. Sci. 441 (1999) 107.

[18] V.R. Dhanak, A.G. Shard, B.C.C. Cowie, A. Santoni, Surf. Sci. 410 (1998) 321.
[19] G. Chen, W.T. Chou, C.T. Yeh, Appl. Catal. 8 (1983) 389.
[20] F.B. Noronha, M. Schmal, M. Primet, R. Frety, Appl. Catal. 78 (1991) 125.
[21] H. Ehwald, V. Leibnitz, Catal. Lett. 38 (1996) 149.
[22] R. Gianantonio, V. Ragaini, P. Magni, J. Catal. 146 (1994) 103.
[23] J.T. Miller, B.L. Meyers, F.S. Modica, G.S. Lane, M. Vaarkamp, D.C. Koningsberger, J. Catal. 143 (1993) 395.
[24] J.T. Miller, B.L. Meyers, M.K. Barr, F.S. Modica, D.C. Koningsberger, J. Catal. 159 (1996) 41.
[25] O. Alexeev, D.W. Kim, G.W. Graham, M. Shelef, B.C. Gates, J. Catal. 185 (1999) 170.
[26] B.E. Spiewak, R.D. Cortright, J.A. Dumesic, J. Catal. 176 (1998) 405.
[27] V.V. Gorodetskii, A.V. Matveev, P.D. Cobden, B.E. Nieuwenhuys, J. Mol. Catal. A: Chem. 158 (2000) 155.
[28] P. Kowalczyk, S. Savard, A. Lasia, J. Electroanal. Chem. 574 (2004) 41.
[29] W.T. Lee, L. Ford, P. Blowers, H.L. Nigg, R.I. Masel, Surf. Sci. 416 (1998) 141.
[30] L.P. Ford, H.L. Nigg, P. Blowers, R.I. Masel, J. Catal. 179 (1998) 163.
[31] A.M. Doyle, S.K. Shaikhutdinov, H.J. Freund, J. Catal. 223 (2004) 444.
[32] U. Muschiol, P.K. Schmidt, K. Christmann, Surf. Sci. 395 (1998) 182.
[33] G.E. Gdowski, T.E. Felter, R.H. Stulen, Surf. Sci. 181 (1987) L147.
[34] M.L. Burke, R.J. Madix, Surf. Sci. 237 (1990) 1.
[35] R.J. Behm, K. Christmann, G. Ertl, Surf. Sci. 99 (1980) 320.
[36] M.G. Cattania, V. Penka, R.J. Behm, K. Christmann, G. Ertl, Surf. Sci. 126 (1983) 382.
[37] P.A. Redhead, Vacuum 12 (1962) 203.
[38] R.J. Cvetanovic, Y. Amenomiya, Adv. Catal. 17 (1967) 103.
[39] R.J. Cvetanovic, Y. Amenomiya, Catal. Rev. 6 (1972) 21.
[40] E. Poulain, V. Bertin, S. Castillo, A. Cruz, J. Mol. Catal. A 116 (1997) 385–396.
[41] B. Hammer, J.K. Nørskov, Nature 376 (1995) 238.